JOURNAL OF GEOPHYSICAL RESEARCH, VOL. 113, B12308, doi:10.1029/2007JB005567, 2008

Mantle Q structure from S-P differential attenuation measurements

Satoko Oki[1,2] and Peter M. Shearer[1]

Received 21 December 2007; revised 31 May 2008; accepted 15 September 2008; published 25 December 2008.

[1] We describe a new one-dimensional Q model for short-period body waves derived from a data set of 15,000 differential t^* measurements of teleseismic P and S waves recorded in broadband seismograms. Measured t^* values are little affected by the source time function or instrument response since the P and S waves are recorded at the same station from the same event. We process the data using a waveform cross-correlation method applied to the first half cycle of the waveforms to avoid reflection and conversion effects. We invert our t^* measurements for a two-layer Q_S model. Our new Q model has about the same attenuation in the upper mantle and less attenuation in the lower mantle than models derived from longer period data sets. This implies that the frequency dependence of Q is more apparent in the lower mantle and that the effects of attenuation in the upper mantle are approximately constant at frequencies below about 1 Hz. We also observe lateral variations of attenuation in the uppermost mantle by solving for station and event terms, which exhibit correlations with regional tectonics.

Citation: Oki, S., and P. M. Shearer (2008), Mantle Q structure from S-P differential attenuation measurements, *J. Geophys. Res.*, *113*, B12308, doi:10.1029/2007JB005567.

1. Introduction

[2] Modeling Earth's anelastic structure as well as elastic structure is important for several reasons: (1) the depth dependence of attenuation and the shear-to-bulk Q ratio constrain the physical state of the deep Earth including its melt content, (2) attenuation can be a good indicator of temperature variations because these variations have a larger effect on attenuation than on elastic velocity, and (3) attenuation causes physical dispersion of seismic velocities, which must be taken into account when interpreting travel time data [e.g., *Gilbert and Dziewonski*, 1975; *Oki et al.*, 2004; S. Oki et al., Reference frequency for waveform-based travel time measurement, manuscript in preparation, 2007]. However, attenuation studies have proven challenging because of the typically large scatter in attenuation measurements and the difficulty in separating out source and elastic propagation effects from the intrinsic attenuation signal.

[3] Early attempts to model global Q structures are derived mainly from low-frequency data sets such as normal modes or surface waves (i.e., PREM [*Dziewonski and Anderson*, 1981]; AK135-Q [*Montagner and Kennett*, 1996]; QL6 [*Durek and Ekström*, 1996]), which were used to solve for average Q values in a layered Earth. Although these models disagree in many of their details, a robust qualitative result has been obtained that most attenuation occurs in the upper mantle and that much less attenuation is observed in the lower mantle. Progress has been slower in modeling high-frequency Q because of the increased importance of scattering and focusing/defocusing effects from 3-D elastic structure. Before recent improvements in the global seismic network, high-frequency data were typically analyzed in regional rather than global studies (e.g., American continents [*Kanamori*, 1967; *Der et al.*, 1982]; Eurasian shield [*Der et al.*, 1986]; Pacific subduction zones [*Sharrock et al.*, 1995a, 1995b]). These results showed that there are distinct lateral Q variations, especially in the upper mantle, associated with tectonic history. For instance, high attenuation is observed at mid-ocean ridges, back-arc basins, and hot spots, whereas the least attenuating regions are in continental interiors or slabs [e.g., *Sipkin and Jordan*, 1980; *Chan and Der*, 1988].

[4] More recently, lateral variations in attenuation have been modeled by applying tomographic methods to surface wave data [e.g., *Billien et al.*, 2000; *Selby and Woodhouse*, 2002; *Gung and Romanowicz*, 2004]. The huge amount of body wave data from global seismic networks now enables seismologists to better model lateral variations of Q at high frequencies. *Bhattacharyya et al.* [1996] analyzed several thousand *SS*-*S* differential waveforms and constrained variations of shear wave attenuation in the upper mantle. *Warren and Shearer* [2000] stacked thousands of P and *PP* spectra and mapped lateral variations in P wave attenuation in the upper mantle. *Lawrence and Wysession* [2006] inverted 30,000 differential *ScS*-*S* attenuation values for a spherically symmetric radial Q model. There is, however, only qualitative agreement among the different models.

[5] Frequency dependence of attenuation has long been indicated by differences between Q observations at high and low frequencies [*Jackson et al.*, 1992; *Anderson and Minster*, 1979]. In particular, less attenuation is observed at 1 Hz than

[1]Institute of Geophysics and Planetary Physics, Scripps Institution of Oceanography, University of California, San Diego, La Jolla, California, USA.

[2]Now at Earthquake Research Institute, University of Tokyo, Tokyo, Japan.

0148-0227/08/2007JB005567$09.00

at long periods ($T > 20$ s). The roll-off in attenuation occurs between about 2 and 10 s and is often modeled with a power law dependence of Q on frequency. *Jackson et al.* [2002] measured grain-size-sensitive shear wave attenuation in the upper mantle at high temperatures and seismic frequencies, and found absorption band viscoelastic behavior with a power law of 0.25. Studies of broadband seismic data have enabled seismologists to test the power law model over a continuous frequency band, rather than discrete frequency values, and have indicated a frequency dependence of Q of $\omega^{0.1-0.4}$ (to ~1 Hz from *Ulug and Berckhemer* [1984]; ~6 Hz from *Cheng and Kennett* [2002]; and ~8.0 Hz from *Shito et al.* [2004]).

[6] Here, we describe a new one-dimensional Q model for short-period body waves on the basis of analysis of a data set of 15,000 differential t^* measurements of teleseismic P and S waves recorded in broadband seismograms; t^* represents the attenuation summed along a raypath and is defined as

$$t^* = \int_{path} \frac{1}{Q} \frac{ds}{c(f_0)}, \tag{1}$$

where c is the velocity, f_0 is the reference frequency of physical dispersion (to be explained later) and $ds/c(f_0)$ is the incremental travel time along the raypath, which can be computed from ray theory from a reference seismic velocity model. We invert our t^* measurements for single to multilayered Q_S models at frequencies that fill a gap between previous long- and short-period studies. We observe too much scatter in our t^* observations to solve reliably for general 3-D attenuation structure, although we observe some lateral variations in uppermost mantle attenuation by solving for station and event terms.

2. Data Processing

[7] We use the broadband data provided by the Incorporated Research Institutions for Seismology (IRIS) through the system of the Fast Archive Recovery Method (FARM), which routinely preassembles the records of earthquakes with magnitudes larger than 5.7 (for events shallower than 100 km) or 5.5 (for deeper events). Several hundred moderate to large events are recorded annually by broadband seismometers that are sensitive to ground velocity in an approximate frequency range from 0.01 to 6 Hz. We measure P on the vertical component and S on the transverse component (after correcting for gain and rotating the two horizontal components). We search for high-quality P and S pairs of seismograms recorded at the same station for estimated turning point depths below 750 km for 5 years from 1998 to 2002.

[8] We measure the differential attenuation of t_S^* and t_P^* (hereafter termed $t_{S\text{-}P}^*$) using waveform cross correlation. We synthesize an S waveform from the observed P wave and cross-correlate it with the observed S waveform. The synthetic waveform can be obtained, in general, by convolving (1) the waveform at the source, (2) the effects of wave propagation throughout the mantle, (3) the effects of reflections and conversions near the source and stations, and (4) the instrument response. We neglect the first and fourth terms in our procedure, since our P and S data are recorded at the same station and from the same source (later we will discuss the effect of possible differences in the P and S corner frequencies). Regarding the third factor, we find that applying a crustal correction can improve the waveform fit, but mostly in the later parts of the waveform. Because we perform our fit using only the first half cycle of the waveform, we do not attempt to perform any crustal corrections (see *Oki et al.* [2004] for the details of the crustal effect).

[9] The wave propagation effects on the waveform include (1) geometrical spreading, (2) multiple arrivals from the upper mantle discontinuities, (3) multipathing due to strong lateral heterogeneity, and (4) attenuation due to internal friction. Geometrical spreading changes only the wave amplitude and can be ignored in our method, since we normalize the wave amplitudes when we cross-correlate them. The second effect can be significant at turning point depths near the transition zone so we limit our analysis to data with turning points deeper than 750 km. The third effect is a source of possible error in many attenuation studies and likely contributes to the large scatter we observe in our measurements. We attempt to minimize its effects by fitting only the first half cycle of the waveforms and by averaging over many different source-receiver paths. We assume that our averaged differential t^* measurements are dominated by the fourth effect, and from this correction we compute the differential attenuation between P and S. Our results are mainly sensitive to periods between about 3 and 10 s, intermediate between LP (>20 s) and short-period (~1 s) studies.

[10] To compute synthetic S waveforms, we convolve our observed P waveforms with a t^* operator derived from a frequency-independent Q model (later we will discuss the implications of frequency-dependent Q on our results). Because we do not consider the absolute traveltime difference between the P and S pulses, but only their relative shapes, this operator can be expressed as

$$A(\omega) = e^{-\omega t^*/2} e^{-i\omega t^* \ln(\omega/\omega_0)/\pi}, \tag{2}$$

where $\omega = 2\pi f$ and the first term gives the amplitude reduction and the second gives the phase shift due to the physical dispersion of velocity. The reference frequency f_0 itself does not bear any physical significance and can be any frequency in the seismic band where the frequency-independent Q is assumed. The difference in Q values between P and S waves is expressed as the difference in t^* (i.e., $t_{S\text{-}P}^*$). Figure 1 shows the synthetic waveforms calculated with various $t_{S\text{-}P}^*$ values from an observed P waveform.

[11] The synthetic waveform broadens as $t_{S\text{-}P}^*$ increases. We obtain the best fitting match between the observed and synthetic waveforms by choosing an appropriate value of $t_{S\text{-}P}^*$. Our misfit measure is given by the cross-correlation coefficient between the observed and synthetic waveforms. To minimize biases from multipathing and other propagation path effects, we perform the cross-correlation only on the first half swing of the waveform. Our fitting method considers $t_{S\text{-}P}^*$ at 1 s increments between 1 and 6 s. While this provides a relatively coarse t^* measure for individual records, note that the scatter in the $t_{S\text{-}P}^*$ observations, even at

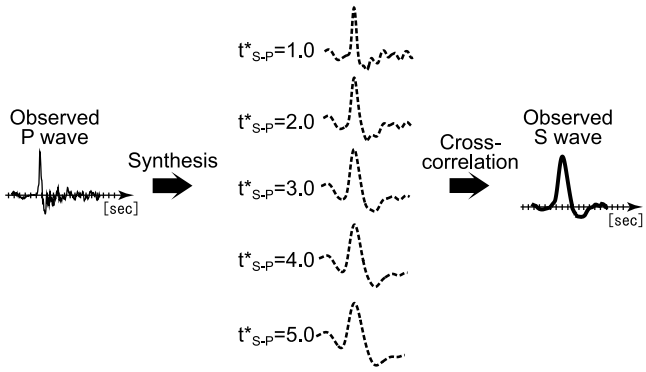

Figure 1. Synthetic S waves derived from an observed P wave using various $t^*_{S\text{-}P}$ values. These synthetic waves are cross-correlated with the observed S wave to find the best fitting $t^*_{S\text{-}P}$ value.

similar source-receiver paths, is much more than 1 s and that stable results are obtained only by averaging many observations. We obtain about 15,000 high-quality $t^*_{S\text{-}P}$ data after visually checking all the cross-correlated waveforms as well as applying a minimum cross-correlation coefficient criteria.

[12] Our observed average $t^*_{S\text{-}P}$ values are almost constant as a function of epicentral distance or of ray turning point depth, as shown in Figure 2 (solid line). Because uniform mantle attenuation would predict increasing $t^*_{S\text{-}P}$ with increasing travel time, this result indicates that mantle attenuation must be stronger at shallow depths.

3. Modeling Q Structure

[13] Assuming that the Q structure is laterally homogeneous and discretely layered in depth, the t^* value, defined as equation (1), can be written as

$$t^* = \sum_j \frac{T_j}{Q_j}, \tag{3}$$

where T_j and Q_j indicate the travel time of the ray and the Q value in the jth layer, respectively. Thus the differential $t^*_{S\text{-}P}$ values in our study may be expressed as

$$t^*_{S-P} = t^*_S - t^*_P = \sum_j \frac{(T_S)_j}{(Q_S)_j} - \sum_j \frac{(T_P)_j}{(Q_P)_j}, \tag{4}$$

where $T_{P,S}$ and $Q_{P,S}$ are the travel time and Q values for P and S waves. We model only Q_S structure by assuming that the bulk attenuation is zero (i.e., that shear attenuation dominates both Q_P and Q_S), in which case

$$Q_P = \frac{9}{4}\, Q_S, \tag{5}$$

for a Poisson solid. Instead of 9/4, we also examined the value of 2.4 which is the predicted average of the ratio for PREM or QL6, and confirmed that the resultant Q models differed by less than 2%.

[14] In this section, we first apply equation (4) to solve for single- to multilayered Q models and discuss the robust features of attenuation in the mantle. Then we consider lateral heterogeneity of attenuation in the uppermost layer by introducing event and station terms.

3.1. Inverting for 1-D Q Structure

[15] With equations (4) and (5), the relation between our $t^*_{S\text{-}P}$ observations and Q_S can be written in matrix form as

$$d_i = T_{ij} q_j, \tag{6}$$

where

$$d_i = (t^*_{S-P})_i, \tag{7}$$

$$T_{ij} = (T_S)_{ij} - \frac{4}{9}(T_P)_{ij}, \tag{8}$$

$$q_j = (Q_S^{-1})_j, \tag{9}$$

and t^*_i, $(T_{P,S})_{ij}$, and $(Q_S^{-1})_j$ denote the ith observation of $t^*_{S\text{-}P}$, the travel time of the ith path in the jth layer, and the Q_S^{-1} value of jth layer, respectively. We iteratively solve equation (6) with the singular value decomposition method. We compute the P and S raypaths and travel times from PREM.

[16] We experiment with calculating Q models for 1 to as many as 16 different layers. We limit the possible boundary depths to discrete values (at about 50 to 150 km depth intervals) set by our ray-tracing code for calculating $(T_{P,S})_{ij}$. As shown in Figure 2, the best fitting one-layer model predicts increasing $t^*_{S\text{-}P}$ with increasing travel time, which is not true for our observed data set. A much better fit is obtained using a two-layer model with the layer boundary at 712 km (slightly larger misfits are obtained when the layer boundary is moved to 630 or 800 km). We parameterize the misfit between the model predictions and the observations

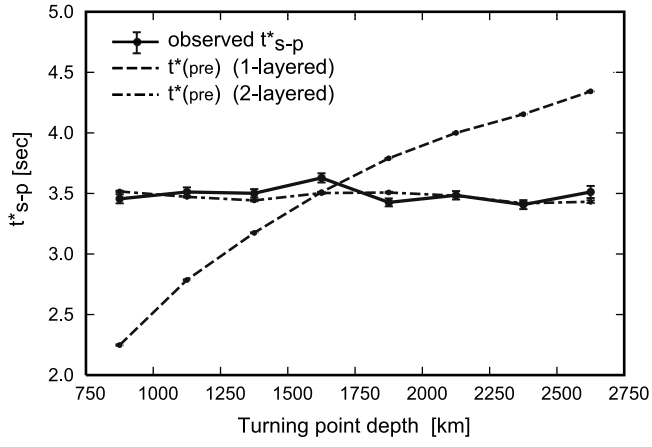

Figure 2. Mean values of observed (solid line) and predicted $t^*_{S\text{-}P}$ binned and averaged at 300 km intervals by ray turning point depth. Dashed and dash-dotted lines are those predicted by the best fitting one- and two-layered models, respectively. Note that the observed values are largely independent of turning depth and that the one-layer model cannot explain the observed t^* values.

Table 1. RMS of Residual $t^*_{S\text{-}P}$ for Mantle Q_S Models With Varying Numbers of Layers

Number of Layer	RMS of $t^*_{(res)}$
1	1.688
2	1.540
3	1.539
8	1.528
16	1.524

using the RMS of the residuals. As shown in Table 1, the RMS misfit is significantly less for the two-layer model compared to the single layer model. The size of the decrease is, however, limited by the 1 to 2 s scatter in the individual $t^*_{S\text{-}P}$ observations. The misfit reduction for the two-layer model is much greater with respect to the binned and averaged points plotted in Figure 2. The results for the 3- to 16-layer Q models do not show much further improvement in fit, regardless of where the layer boundaries are placed. Thus, we will only consider the two-layer model for the remainder of this paper.

[17] The derived Q_S values are shown in Table 2 and Figure 3 (solid line) plotted together with PREM (dotted line) for reference. Compared with PREM, our model shows about the same attenuation in the upper mantle but much less attenuation in the lower mantle. We discuss these features later in terms of the frequency dependence of Q values.

[18] Our method assumes that the P and S wave spectral properties are the same at the source. However, there is some evidence that P wave corner frequencies are higher than S wave corner frequencies, which could bias our results. The biasing effect would depend on the position of the corner frequency with respect to the bandwidth of our data. Because corner frequencies vary systematically as a function of earthquake size, this effect might show up as a magnitude dependence in our data. We tested for this possibility by examining our $t^*_{S\text{-}P}$ observations versus moment magnitude (Figure 4). We observe a positive correlation between $t^*_{S\text{-}P}$ and moment for $M_W < 6.8$ and a drop in $t^*_{S\text{-}P}$ for larger events. We test the importance of this effect by examining how the resultant Q_S model changes by correcting the $t^*_{S\text{-}P}$ values using a line fit to Figure 4 to that of Mw 6.0. The resultant Q_S values for the lower mantle increase slightly from 622 to 650 but little change is observed for the upper mantle. We conclude that our Q_S model is robust with respect to earthquake size bias effects.

3.2. Event and Station Terms

[19] Previous studies have shown large regional differences in the strength of upper mantle attenuation. Our data do not have the raypath coverage to solve for a general model of these variations. However, we can explore some of the first-order differences by computing source and station terms, which describe how much of the 3-D attenuation signal can be explained by near-source or near-receiver Q structure. Here we adopt the iterative approach used by *Warren and Shearer* [2002] to solve for these terms. This method takes advantage of the large size of our data set, with many sources for each receiver and many receivers for each source.

[20] In this case, equation (6) becomes

$$d_i = T_{ij} q_j + E_{ik} e_k + S_{il} s_l, \tag{10}$$

where

$$E_{ik} = 1 \quad \text{when observation is from event } k, \tag{11}$$

$$E_{ik} = 0 \quad \text{otherwise}, \tag{12}$$

$$S_{il} = 1 \quad \text{when observation is from station } l, \tag{13}$$

$$S_{il} = 0 \quad \text{otherwise}. \tag{14}$$

e_k and s_l are the event and station terms for the kth event and lth station, respectively. For the first iteration, we set e_k and s_l to zero and solve for $(Q_S^{-1})_j$ as in section 3.1. We then estimate e_k for each event as the average of the residuals between the observed and predicted t^* values from other model parameters:

$$e_k = \frac{1}{ns_k} \sum_i E_{ik} t^*_{i\,(res)} = \frac{1}{ns_k} \sum_i E_{ik} [d_i - T_{ij} q_j - S_{il} s_l], \tag{15}$$

where ns_k is the number of stations recording the lth event. Similarly, we estimate s_l for each station as

$$s_l = \frac{1}{ne_l} \sum_i S_{il} t^*_{i\,(res)} = \frac{1}{ne_l} \sum_i S_{il} [d_i - T_{ij} q_j - E_{ik} e_k], \tag{16}$$

where ne_l is the number of events recorded by the lth station. Following the updated event and station term

Table 2. Q_S Values for Two-Layered Models Without and With Event and Station Terms

Depth	Q_S Without Terms	Q_S With Terms
0–712	100	101
712–2900	645	621

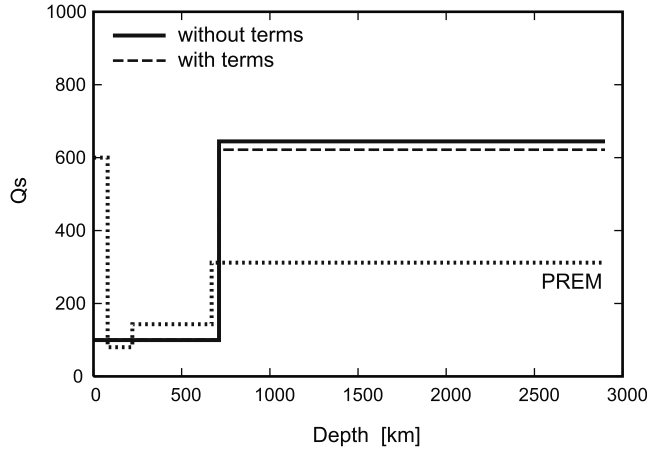

Figure 3. Derived Q_S models plotted together with that of PREM as a reference (dotted line). Solid and dashed lines indicate models computed without and with event and station terms, respectively. Compared with PREM, our Q_S models have almost the same attenuation in the upper mantle and much less attenuation in the lower mantle.

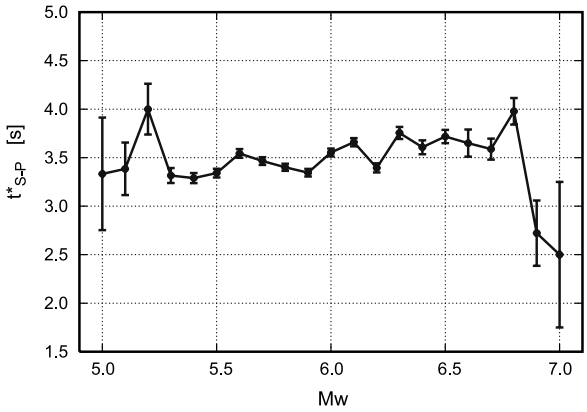

Figure 4. Observed $t^*_{S\text{-}P}$ values binned and averaged as a function of moment magnitude.

estimates, we solve for $(Q_S^{-1})_j$ using equations (10) and continue iterating using (10), (15), and (16) until a stable set of $(Q_S^{-1})_j$, e_k, s_l are obtained. We find in practice that this method converges after only two or three iterations.

[21] The resultant Q_S values for the two-layered model remain largely unchanged as shown in Figure 3 (dashed line) and Table 2, even though the variance of residual $t^*_{S\text{-}P}$ relative to predicted $t^*_{S\text{-}P}$ reduces from 2.37 to 1.30 with the event and station terms. We obtain 870 event terms and 605 station terms, which are plotted as histograms in Figure 5 and in map view in Figure 6. We see more variation in the event terms than in the station terms, consistent with the P wave spectral results of *Warren and Shearer* [2002].

[22] In Figure 6, positive values of event terms are seen along the mid-ocean ridges. This can be explained by the tectonic setting of ocean ridges where hot material with possible partial melt exists. It has been observed that earthquakes on oceanic transforms tend to have slow ruptures [e.g., *Kanamori and Stewart*, 1976; *Okal and Stewart*, 1982; *Ekström and Dziewonski*, 1988; *Shearer*, 1994; *Kaverina et al.*, 1996; *Choy and McGarr*, 2002], but this should not affect our data set since we use only differential P and S waveform measurements.

[23] The patterns of t^* terms at stations tend to show regional tectonic differences. In Figures 7a and 7b, close-ups of North America and the southern part of Africa are shown. The tendency that positive attenuation is observed in the Basin and Range and that less attenuation is seen in the eastern United States and at Yellowstone is consistent with previous studies [e.g., *Patton and Taylor*, 1984; *Lay and Wallace*, 1988; *Artemieva et al.*, 2004; *Lawrence et al.*, 2006]. The relatively weak attenuation in the southern part of Africa was also detected by the tomographic Q study of *Selby and Woodhouse* [2002] and may reflect the tectonically stable Precambrian shield.

[24] Using *Warren and Shearer*'s [2002] auxiliary material via ftp site, we compared their event and station terms derived from P waves (t^*_P) to those of ours ($t^*_{S\text{-}P}$) by picking those in common. To better constrain the comparison, we required their event and station terms to have more than 20 stations and 30 events, respectively. Figure 8 shows the $t^*_{S\text{-}P}$ values plotted against t^*_P. Although the results exhibit consider scatter, the two data sets are clearly correlated. We calculate the slope by least squares fitting with errors in both axes. We weight the x and y axes misfit by the square root of the observed earthquake or station numbers, i.e., $\sqrt{n_P}$ for the x axis and $\sqrt{n_{SP}}$ for the y axis for each data point. The slope is estimated as 4.4 ± 0.5 (solid line). For a Poisson solid with all attenuation in shear, we expect $t_S^* = (9\sqrt{3}/4)t_P^* \simeq 4t_P^*$, in which case the expected ratio of $t^*_{S\text{-}P}$ to t^*_P is 3, somewhat less than our observed value. However, the *Warren and Shearer* [2002] results are from a higher

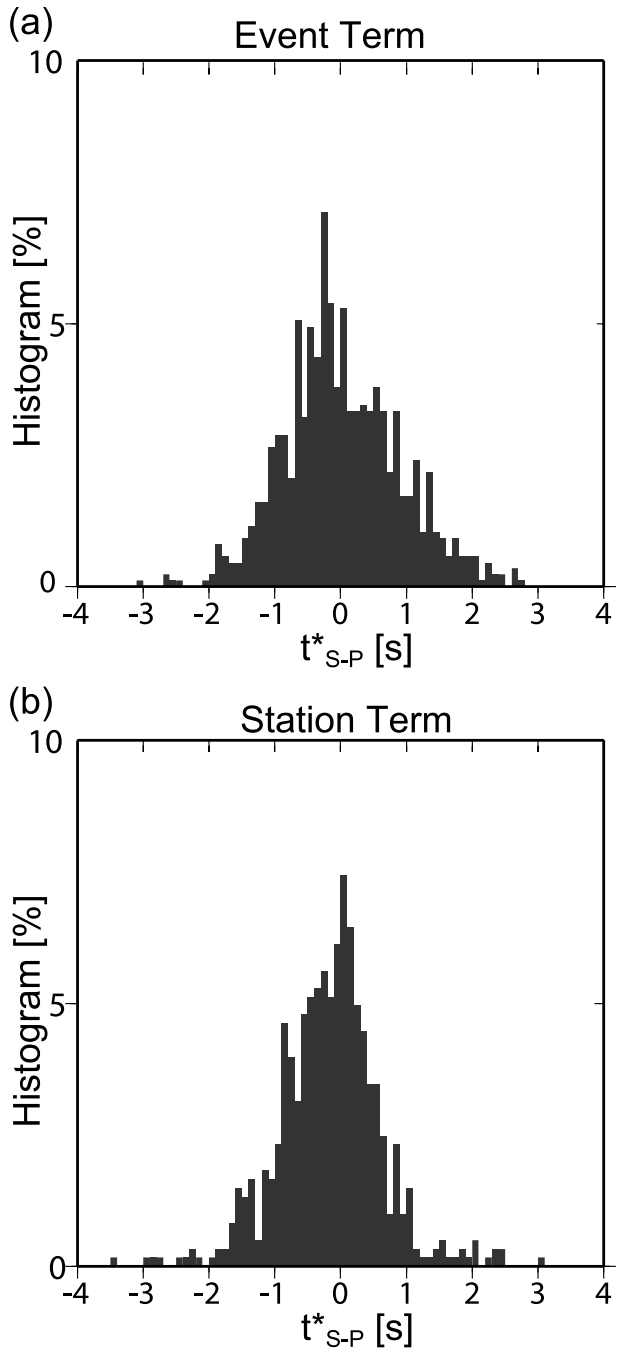

Figure 5. Histograms of (a) event and (b) station attenuation terms. Note the greater variation in the earthquake terms compared to the station terms.

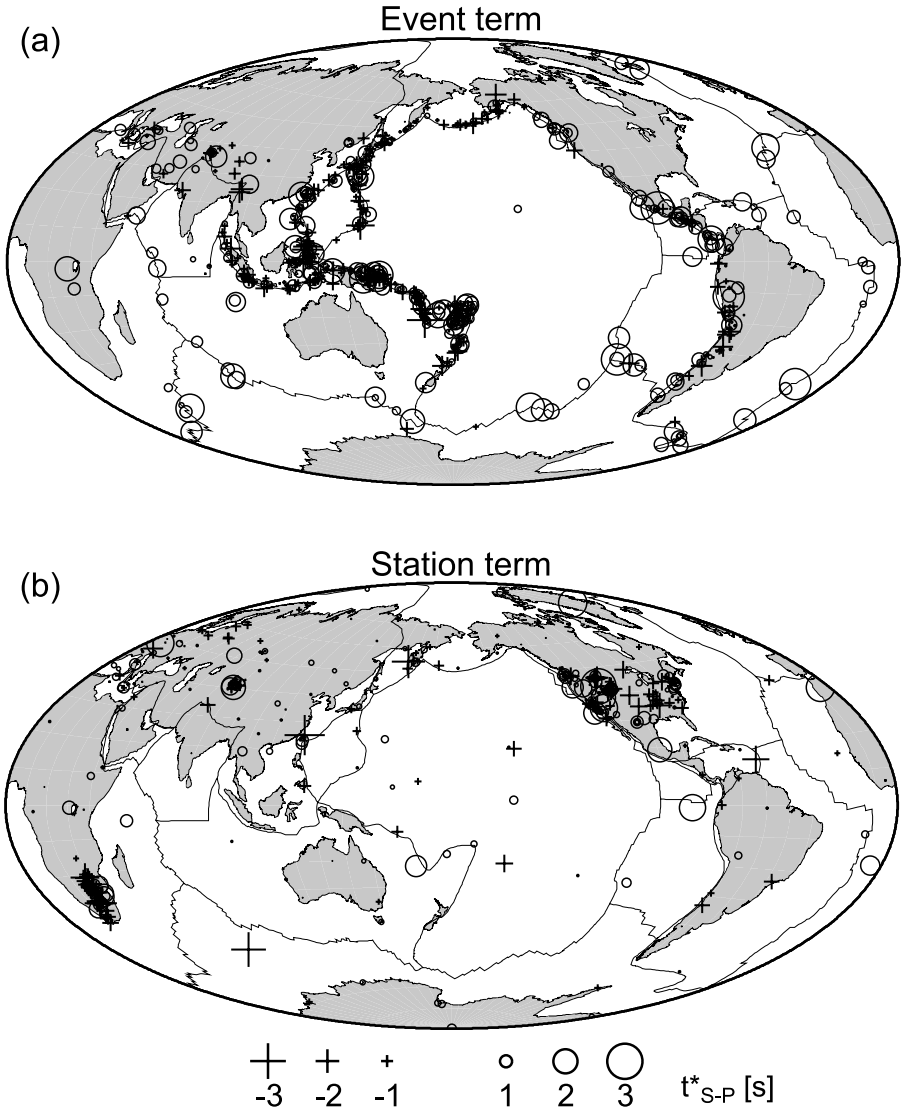

Figure 6. Maps of (a) event and (b) station terms. Symbol size scales with $t^*_{S\text{-}P}$ as indicated. Positive values are seen along the mid-ocean ridges (Figure 6a).

frequency band, where less attenuation is expected than at the band of our observations. This effect would tend to make the slope larger than the value near 3 expected from t^*_P and $t^*_{S\text{-}P}$ measurements at the same frequency.

3.3. Three-Dimensional Distribution of Q_S

[25] In principle, we could derive three-dimensional Q structure with our $t^*_{S\text{-}P}$ data set, although much of the lateral variability in upper mantle attenuation is absorbed into our event and station terms. To test whether there are spatially coherent variations in lower mantle attenuation, we plotted $t^*_{S\text{-}P}$ residuals (computed with the event and station terms) at the bottoming points of the source-receiver raypaths. These plots showed large scatter and little spatial coherence, without clear patterns of high- and low-attenuation regions. We experimented with implementing azimuthally dependent event and station terms (i.e., by computing separate terms for four different back azimuth directions) but found little reduction in misfit variance or any improved spatial coherence in the residuals. These results imply that there is little measurable contribution to our observed $t^*_{S\text{-}P}$ data from large-scale 3-D variations in lower mantle attenuation. On the basis of our one-dimensional Q model, both P and S waves observed at 60 from a surface source spend about 33% of their times in the upper mantle while accumulating 78% of their t^*, similar to results discussed by *Warren and Shearer* [2002]. These results indicate that t^* observations are not very sensitive to variations in attenuation in the lower mantle, at least for short-period body waves.

4. Frequency Dependence of Q

[26] A weak frequency dependence of Q^{-1} is suggested by body wave studies [*Sipkin and Jordan*, 1979; *Ulug and Berckhemer*, 1984; *Shito et al.*, 2004]. Those studies show a dependence of Q^{-1} at frequencies between 0.1 and 8.0 Hz with a power law of f^{α}, where α varies from 0.1 to 0.4, as well as the experimental studies in the seismic frequency

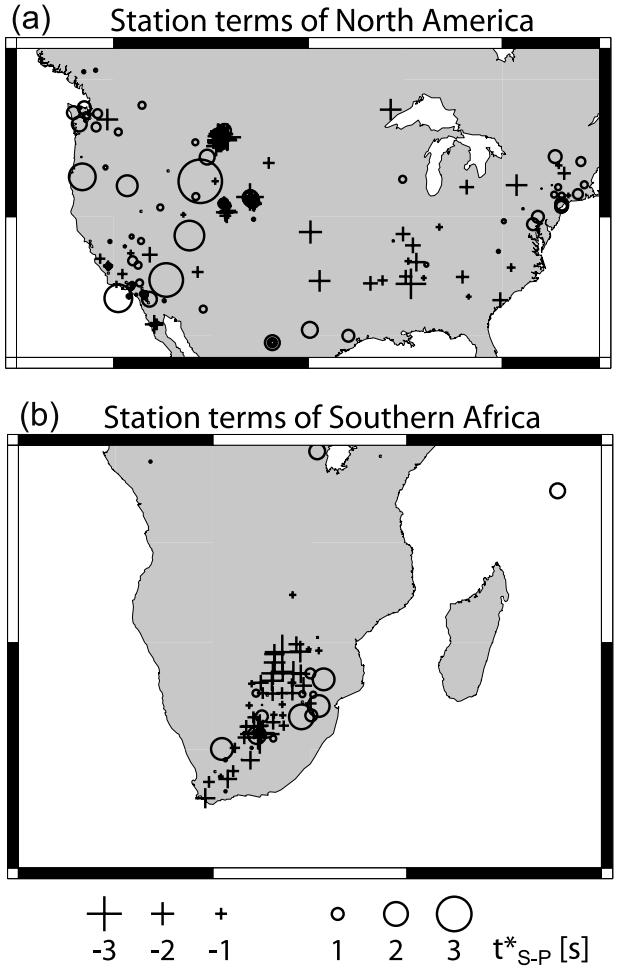

Figure 7. Maps of regional close-ups of station terms in (a) North America and (b) the southern part of Africa. Symbol size scales with $t^*_{S\text{-}P}$ as indicated. Positive values are seen in the Basin and Range (Figure 7a), whereas less attenuation is seen in the eastern United States and at Yellowstone (Figure 7a) and in the southern part of Africa (Figure 7b).

band [*Jackson et al.*, 2002]. In our study, we do not attempt to estimate α, but we plot various Q models, including our own, against frequency to see the overall trend of mantle attenuation versus frequency. We do not try to resolve the frequency dependence of Q directly in our data, but instead compare our results with other Q studies conducted at different frequencies. This raises the question as to whether our results may be biased by our assumption of constant Q in our $t^*_{S\text{-}P}$ modeling if Q is significantly frequency-dependent over the roughly 3–10 s band of our data. To test this, we computed synthetic seismograms based on an absorption band model [*Lundquist and Cormier*, 1980; *Doornbos*, 1983], in which the t^* operator is given by

$$\exp\left\{\frac{-\omega t^*}{\pi}\tan^{-1}\left[\frac{\omega(\tau_2-\tau_1)}{1+\omega^2\tau_1\tau_2}\right]-\frac{i\omega t^*}{2\pi}\ln\left[\frac{1+1/\omega^2\tau_1^2}{1+1/\omega^2\tau_2^2}\right]\right\}, \quad (17)$$

where τ_1 and τ_2 are the lower and upper relaxation times that describe the edges of the absorption band. Note that the corresponding lower frequency limit is given by $f_1 = 1/2\pi\tau_2$ and the upper frequency limit by $f_2 = 1/2\pi\tau_1$. Approximating the two-layer Q model of *Warren and Shearer* [2000], we assumed an upper mantle with frequency-independent Q characterized by $t^*_P = 0.4$ and $t^*_S = 1.6$, and a lower mantle with frequency-dependent Q described by $f_1 = 0.001$ Hz, $f_2 = 0.8$ Hz, and $t^*_P = 0.6$ and $t^*_S = 2.4$ (low-frequency limits). We assumed a source time function of the form

$$A(f) = \frac{\Omega_0}{1+(f/f_c)^2}, \quad (18)$$

where Ω_0 is the low-frequency spectral level and f_c is the corner frequency. We set $f_c = 0.2$ Hz, which is typical of $M_W = 6$ earthquakes. Using the constant Q assumption of our analysis method (i.e., equation (2)), we obtained a best fitting $t^*_{S\text{-}P}$ of 2.8 s (computed to a precision of 0.1 s), which is close to the low-frequency prediction of our assumed model. This test suggests that our assumption of constant Q in our $t^*_{S\text{-}P}$ modeling produces reasonable results over the roughly 3–10 s band of our data, even if Q actually has some frequency dependence over this band.

[27] Our model helps fill in a rather sparse band of observations at high frequencies, especially for the lower mantle because many of the high-frequency data sets sampling the deep mantle are limited to core-reflected

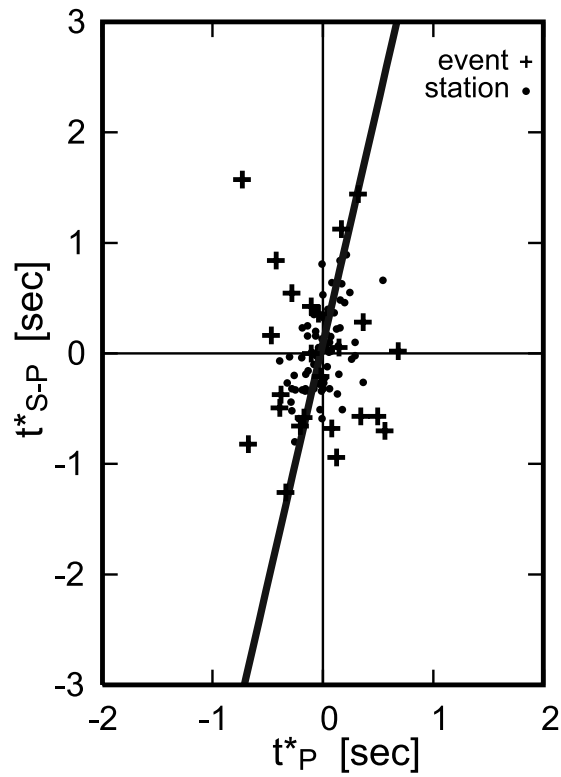

Figure 8. Comparison of the event and station terms from *Warren and Shearer* [2002] (t^*_P) and this study ($t^*_{S\text{-}P}$). To better constrain the comparison, we required their event and station terms to have more than 20 stations (solid circle) and 30 events (cross), respectively. The solid line with a slope of 4.4 shows the least squares fit assuming errors in both axes.

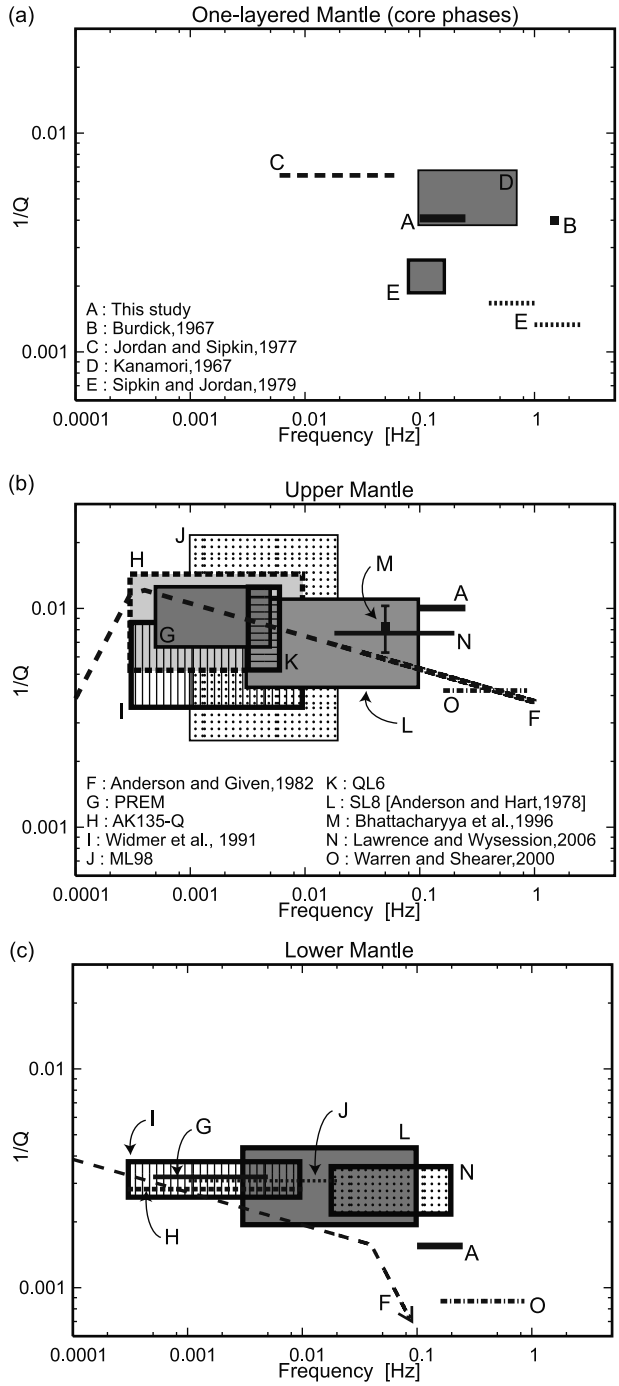

Figure 9. Various Q_S models plotted against the frequency bands of the data sets for (a) a one-layered mantle, (b) the upper mantle, and (c) the lower mantle. Note that the Q_S values for the upper mantle do not depend on frequency for the models at <1 Hz, whereas frequency dependence is seen in the lower mantle. (models: A, this study; B, *Burdick* [1985]; C, *Jordan and Sipkin* [1977]; D, *Kanamori* [1967]; E, *Sipkin and Jordan* [1979]; F, *Anderson and Given* [1982]; G, PREM [*Dziewonski and Anderson*, 1981]; H, AK135-Q [*Montagner and Kennett*, 1996]; I, *Widmer et al.* [1991]; J, ML98; K, QL6 [*Durek and Ekström*, 1996]; L, SL8 [*Anderson and Hart*, 1978]; M, *Bhattacharyya et al.* [1996]; N, *Lawrence and Wysession* [2006]; O, *Warren and Shearer* [2000]).

phases, which have difficulty in distinguishing attenuation between the upper and lower mantle. Global Q models are well constrained with longer-period data. PREM, AK135-Q, and *Widmer et al.* [1991] use normal modes, QL6 uses long-period Rayleigh and Love waves in addition to normal modes, and ML98 (G. Masters, personal communication, 2007) uses normal modes, surface waves and long-period body waves. These long-period Q models are generally consistent with each other, especially in the lower mantle. Before the improvement of the global seismic network, Q models from body waves were generally limited to regional studies, which mainly used core-reflected phases (Americas [*Kanamori*, 1967] and western Pacific [*Jordan and Sipkin*, 1977, *Sipkin and Jordan*, 1979, *Sharrock et al.*, 1995a, 1995b]). These studies derived averaged Q values throughout whole mantle.

[28] *Anderson and Hart* [1978] made an effort to construct a model satisfying body wave, surface wave and normal-mode data. The model, *SL8*, has increasing Q values in the lowermost mantle. *Anderson and Given* [1982] applied a simple absorption band model to normal-mode, surface and body wave data to constrain the frequency dependence of Q and obtained an α value of 0.15.

[29] More recent studies have used the global seismic network to model detailed global Q structure from body waves. *Bhattacharyya et al.* [1996] analyzed *SS-S* differential waveforms of 20 s dominant period to constrain the lateral variation of shear wave attenuation in the upper mantle. *Lawrence and Wysession* [2006] inverted differential *ScS-S t** for a spherically symmetric radial model of Q_S with high sensitivity to the lower mantle. *Warren and Shearer* [2000, 2002] used globally distributed *P* and *PP* waves to examine short-period Q_P and its lateral variability in the upper mantle.

[30] These previous results are summarized and compared to our $t^*_{S\text{-}P}$ results in Figure 9a for a one-layered mantle, Figure 9b for the upper mantle, and Figure 9c for the lower mantle. We use our one-layered Q model for the case of Figure 9a, and our two-layered model for Figures 9b and 9c. We apply our relation of Q_P and Q_S in equations (5) and plot them in terms of Q_S^{-1} for those models provided with Q_P.

[31] In interpreting Figure 9a, note that Q values other than those from *Burdick* [1985] (model B in Figure 9) and this study (model A) are derived with regionally restricted data sets. Results from *Kanamori* [1967] (model D) are for the Americas, whereas others (models C and E) are for the western Pacific. Yet the frequency dependence of Q_S^{-1} is implied when taking into consideration that *Sipkin and Jordan* [1979] (model E) used data recorded by both long- and short-period seismometers at the same station and that the study area is the same as that of *Jordan and Sipkin* [1977] (model C).

[32] For the upper and lower Q values, we plot only global studies. Each model has large variance in Q values for the upper mantle, which may reflect large differences in the asthenosphere properties. From Figure 9b, frequency dependence is not obvious in the upper mantle. Rather, the upper mantle can be characterized as a uniformly attenuating layer for data at frequency bands less than 1.0 Hz. On the other hand, frequency dependence is suggested in the lower mantle (Figure 9c). This difference between the upper and lower mantle is consistent with previous studies such as

those by *Choy and Cormier* [1986] and *Warren and Shearer* [2000], and with recent experimental studies [*Jackson et al.*, 2004; *Faul et al.*, 2004] that show that the existence of partial melt weakens the frequency dependence of Q, as partial melt is much more likely in the upper mantle than the lower mantle.

5. Summary

[33] We model one-dimensional shear Q by using differential t^* measurements of teleseismic P and S waves at several to ten seconds period. We process the data using a waveform cross-correlation method applied to the first half cycle of the waveforms. The resulting Q_S model has about the same attenuation in the upper mantle and much less attenuation in the lower mantle when compared to conventional Q models from long-period data sets such as PREM, AK135-Q or QL6. This implies that the frequency dependence of Q is more apparent in the lower mantle and that the effects of attenuation in the upper mantle are approximately constant at frequencies below about 1 Hz. Station $t^*_{S\text{-}P}$ terms exhibit differences correlated with regional tectonics, with strong attenuation in the Basin and Range province of North America and less attenuation in the eastern part of the North America and in the southern part of Africa. Positive values of earthquake $t^*_{S\text{-}P}$ terms are consistently seen along the mid-ocean ridges, suggesting increased attenuation in the shallow underlying mantle.

[34] **Acknowledgments.** We thank Linda Warren for making her data available to us. We also thank Vernon Cormier and an anonymous reviewer for their helpful and constructive comments.

References

Anderson, D. L., and J. W. Given (1982), Absorption band Q model for the Earth, *J. Geophys. Res.*, *87*, 3893–3904.

Anderson, D. L., and R. S. Hart (1978), Q of the Earth, *J. Geophys. Res.*, *83*, 5869–5882.

Anderson, D. L., and J. B. Minster (1979), The frequency dependence of Q in the Earth and implications for mantle rheology and Chandler wobble, *Geophys. J. Int.*, *58*, 431–440.

Artemieva, I. M., M. Billien, J.-J. Lévêque, and W. D. Mooney (2004), Shear wave velocity, seismic attenuation, and thermal structure of the continental upper mantle, *Geophys. J. Int.*, *157*, 607–628.

Bhattacharyya, J., G. Masters, and P. Shearer (1996), Global lateral variations of shear wave attenuation in the upper mantle, *J. Geophys. Res.*, *101*, 22,273–22,289.

Billien, M., J. J. Lévêque, and J. Trampert (2000), Global maps of Rayleigh wave attenuation for periods between 40 and 150 seconds, *Geophys. Res. Lett.*, *27*, 3619–3622.

Burdick, L. J. (1985), Estimation of the frequency dependence of Q from *ScP* and *ScS* phases, *Geophys. J.R. Astron. Soc.*, *80*, 35–55.

Chan, W., and Z. A. Der (1988), Attenuation of multiple *ScS* in various parts of the world, *Geophys. J. Int.*, *92*, 303–314.

Cheng, H.-X., and B. L. N. Kennett (2002), Frequency dependence of seismic wave attenuation in the upper mantle beneath the Australian region, *Geophys. J. Int.*, *150*, 45–57, doi:10.1046/j.1365-246X.2002.01677.x.

Choy, G. L., and V. F. Cormier (1986), Direct measurement of the mantle attenuation operator from broadband P and S waveforms, *J. Geophys. Res.*, *91*, 7326–7342.

Choy, G. L., and A. McGarr (2002), Strike-slip earthquakes in the oceanic lithosphere: observations of exceptionally high apparent stress, *Geophys. J. Int.*, *150*, 506–523.

Der, Z. A., W. D. Rivers, T. W. McElfresh, and A. O'Donnell (1982), An investigation of the regional variations and frequency dependence of anelastic attenuation in the mantle under the United States in the 0.5–0.4 Hz band, *Geophys. J.R. Astron. Soc.*, *69*, 67–99.

Der, Z. A., A. C. Lees, V. F. Cormier, and L. M. Anderson (1986), Frequency dependence of Q in the mantle underlying the shield areas of Eurasia, part I, Analyses of short and intermediate period data, *Geophys. J.R. Astron. Soc.*, *87*, 1057–1084.

Doornbos, D. J. (1983), Observable effects of the seismic absorption band in the Earth, *Geophys. J. Int.*, *75*, 693–711.

Durek, J. J., and G. Ekström (1996), A radial model of anelasticity consistent with long-period surface-wave attenuation, *Bull. Seismol. Soc. Am.*, *86*, 144–158.

Dziewonski, M. A., and D. L. Anderson (1981), Preliminary reference Earth model, *Phys. Earth Planet. Inter.*, *25*, 297–356.

Ekström, G., and A. M. Dziewonski (1988), Evidence of bias in estimations of earthquake size, *Nature*, *332*, 319–323.

Faul, U. H., J. D. Fitz Gerald, and I. Jackson (2004), Shear wave attenuation and dispersion in melt-bearing olivine polycrystals: 2. Microstructural interpretation and seismological implications, *J. Geophys. Res.*, *109*, B06202, doi:10.1029/2003JB002407.

Gilbert, J. F., and A. M. Dziewonski (1975), Application of normal mode theory to the retrieval of structural parameters and source mechanisms from seismic spectra, *Philos. Trans. R. Soc.*, *278*, 187–269.

Gung, Y., and B. Romanowicz (2004), Q tomography of the upper mantle using three-component long-period waveforms, *Geophys. J. Int.*, *157*, 813–830, doi:10.1111/j.1365-246X.2004.02265.x.

Jackson, I., M. S. Paterson, and J. D. Fitz Gerald (1992), Seismic wave dispersion and attenuation in Åheim dunite: An experimental study, *Geophys. J. Int.*, *108*, 517–534.

Jackson, I., J. D. Fitz Gerald, U. H. Faul, and B. H. Tan (2002), Grain-size-sensitive seismic wave attenuation in polycrystalline olivine, *J. Geophys. Res.*, *107*(B12), 2360, doi:10.1029/2001JB001225.

Jackson, I., U. H. Faul, J. D. Fitz Gerald, and B. H. Tan (2004), Shear wave attenuation and dispersion in melt-bearing olivine polycrystals: 1. Specimen fabrication and mechanical testing, *J. Geophys. Res.*, *109*, B06201, doi:10.1029/2003JB002406.

Jordan, T. H., and S. A. Sipkin (1977), Estimation of the attenuation operator for multiple *ScS* waves, *Geophys. Res. Lett.*, *4*, 167–170.

Kanamori, H. (1967), Spectrum of short-period core phases in relation to the attenuation in the mantle, *J. Geophys. Res.*, *72*, 2181–2186.

Kanamori, H., and G. S. Stewart (1976), Mode of strain release along the Gibbs Fracture Zone, Mid-Atlantic Ridge, *Phys. Earth Planet. Inter.*, *11*, 312–332.

Kaverina, A. N., A. V. Lander, and A. G. Prozorov (1996), Global creepex distribution and its relation to earthquake-source geometry and tectonic origin, *Geophys. J. Int.*, *125*, 249–265.

Lawrence, J. F., and M. E. Wysession (2006), QLM9: A new radial quality factor (Q_μ) model for the lower mantle, *Earth Planet. Sci. Lett.*, *241*, 962–971.

Lawrence, J. F., P. Shearer, and G. Masters (2006), Mapping attenuation beneath North America using waveform cross-correlation and cluster analysis, *Geophys. Res. Lett.*, *33*, L07315, doi:10.1029/2006GL025813.

Lay, T., and T. C. Wallace (1988), Multiple *ScS* attenuation and travel times beneath western North America, *Bull. Seismol. Soc. Am.*, *78*, 2041–2061.

Lundquist, G. M., and V. C. Cormier (1980), Constraints on the absorption band model of Q, *J. Geophys. Res.*, *85*, 5244–5256.

Montagner, J. P., and B. L. N. Kennett (1996), How to reconcile body-wave and normal-mode reference earth models, *Geophys. J. Int.*, *125*, 229–248.

Okal, E. A., and L. M. Stewart (1982), Slow earthquakes along oceanic fracture zones: Evidence for asthenospheric flow away from hotspots?, *Bull. Seismol. Soc. Am.*, *80*, 1934–1950.

Oki, S., Y. Fukao, and M. Obayashi (2004), Reference frequency of teleseismic body waves, *J. Geophys. Res.*, *109*, B04304, doi:10.1029/2003JB002821.

Patton, H. J., and S. R. Taylor (1984), Q structure of the Basin and Range from surface waves, *J. Geophys. Res.*, *89*, 6929–6940.

Selby, N. D., and J. H. Woodhouse (2002), The Q structure of the upper mantle: Constraints from Rayleigh wave amplitudes, *J. Geophys. Res.*, *107*(B5), 2097, doi:10.1029/2001JB000257.

Sharrock, D. S., I. G. Main, and A. Douglas (1995a), Observations of Q from the northwest Pacific subduction zone recorded at teleseismic distances, *Bull. Seismol. Soc. Am.*, *85*, 237–253.

Sharrock, D. S., I. G. Main, and A. Douglas (1995b), A two-layer attenuation model for the upper mantle at short-periods, *Geophys. Res. Lett.*, *22*, 2561–2564.

Shearer, P. (1994), Global seismic event detection using a matched filter on long-period seismograms, *J. Geophys. Res.*, *99*, 13,713–13,725.

Shito, A., S. Karato, and J. Park (2004), Frequency dependence of Q in Earth's upper mantle inferred from continuous spectra of body waves, *Geophys. Res. Lett.*, *31*, L12603, doi:10.1029/2004GL019582.

Sipkin, S. A., and T. H. Jordan (1979), Frequency dependence of Q_{ScS}, *Bull. Seismol. Soc. Am.*, *69*, 1055–1079.

Sipkin, S. A., and T. H. Jordan (1980), Regional variation of Q_{ScS}, *Bull. Seismol. Soc. Am.*, *70*, 1071–1102.

Ulug, A., and H. Berckhemer (1984), Frequency dependence of Q for seismic body waves in the Earth's mantle, *J. Geophys.*, *56*, 9–19.

Warren, L. M., and P. Shearer (2000), Investigating the frequency dependence of mantle Q by stacking P and PP spectra, *Geophys. Res. Lett.*, *105*, 25,391–25,402.

Warren, L. M., and P. M. Shearer (2002), Mapping lateral variations in upper mantle attenuation by stacking P and PP spectra, *J. Geophys. Res.*, *107*(B12), 2342, doi:10.1029/2001JB001195.

Widmer, R., G. Masters, and F. Gilbert (1991), Spherically symmetric attenuation within the Earth from normal mode data, *Geophys. J. Int.*, *104*, 541–553.

S. Oki, Earthquake Research Institute, University of Tokyo, Tokyo-to, Bunkyo-ku, Yayoi 1-1-1, Tokyo 113-0032, Japan. (oki@eri.u-tokyo.ac.jp)

P. M. Shearer, IGPP 0225, Scripps Institution of Oceanography, University of California, San Diego, La Jolla, CA 92093-0225, USA.